Effect of the fluid-wall interaction on freezing of confined fluids: Toward the development of a global phase diagram

Ravi Radhakrishnan and Keith E. Gubbins
North Carolina State University, 113 Riddick Labs Raleigh, North Carolina 27695-7905

Malgorzata Sliwinska-Bartkowiak
Instytut Fizyki, Uniwersytet im Adama Mickiewicza, Umultowska 85, 61-614 Poznan, Poland

(Received 28 December 1999; accepted 6 March 2000)

We report molecular simulation studies of the freezing behavior of fluids in nano-porous media. The effect of confinement is to induce spatial constraints as well as energetic heterogeneity on the confined fluid, thereby altering the bulk phase behavior drastically. We consider the effect of the fluid-wall interaction energy on the shift of the freezing temperature and on the fluid structure, using a novel approach to calculate the free energy surface based on Landau theory and order parameter formulation. Corresponding states theory is then used to map out the global freezing behavior of a Lennard-Jones (LJ) fluid in model slit-shaped pores of varying fluid-wall interaction strengths. Using LJ parameters fitted to thermophysical property behavior, we predict the qualitative freezing behavior for a variety of fluids and nano-porous materials, based on a global freezing diagram. We have attempted to verify these predictions by comparing with experimental data for several systems, and show that in these cases, the experimental observations and the predictions are in agreement. © *2000 American Institute of Physics.* [S0021-9606(00)50121-4]

I. INTRODUCTION

Numerous experimental studies have been reported for freezing of fluids in pores.[1–17] Most of the studies[1–17] using silica-based porous materials show a depression of the freezing temperature when compared with the bulk ($\Delta T_f = T_{f,\text{pore}} - T_{f,\text{bulk}} < 0$). For a porous medium with an average pore size that is much greater than the size of the fluid molecules (large pore limit), the Gibbs–Thomson equation,[18] relates the shift in the freezing temperature (ΔT_f) to the average pore diameter (H) and the surface tensions of the pore wall with the confined fluid (γ_{wl}) and the confined solid (γ_{ws}). The Gibbs–Thomson equation is the freezing analogue of the Kelvin equation for condensation, and is based on classical thermodynamics. Experiments done on silica-based pores followed a linear relationship between ΔT_f and $1/H$ in accordance with the Gibbs–Thomson equation, in the limit of large pores. For a particular range of values of γ_{wl} and γ_{ws}, the Gibbs–Thomson equation predicts an elevation in freezing temperature of the confined fluid ($\Delta T_f > 0$). This possibility was investigated in a simulation study that looked at the effect of confinement on freezing of simple fluids in slit pores by Miyahara and Gubbins.[19] Miyahara and Gubbins studied freezing of the Lennard-Jones (LJ) methane in slit-shaped pores with different pore-wall interactions. The authors defined ''attractive pores'' as those for which the potential energy of interaction of the pore wall with the confined fluid is *more attractive* than the potential energy of interaction that would result if the pore wall were to be made up of the solid phase of the fluid molecules that are confined; ''repulsive pores'' were defined as those in which the inverse is true. Their study found that the hysteresis freezing temperature was *increased* for attractive pores and *lowered* for repulsive pores, relative to the bulk material. The hysteresis freezing temperature, as opposed to the thermodynamic freezing temperature, is defined as the limit of metastability of the liquid phase during freezing. Maddox and Gubbins[20] studied freezing and melting of simple fluids in pores of cylindrical geometry, and reached similar conclusions. However, they found important differences because of the increased confinement in a cylindrical geometry. In particular, the additional confinement led to downward shifts in the freezing temperatures when compared to confinement in a slit geometry. The predictions of Miyahara and Gubbins were confirmed by rigorous free energy studies, in which the thermodynamic freezing temperature in confined systems was calculated.[21,22] These studies also established that the freezing transition was first order in such confined systems.

Recently, Kaneko *et al.*[23,24] studied freezing of CCl_4 in activated carbon fibers using differential scanning calorimetry (DSC), and reported an elevation in T_f for the confined system, thus verifying the prediction made by simulations.[19,22] The authors argued that, due to the high density of covalently bonded carbon atoms in graphite, the fluid-wall interaction is large and hence the observation is consistent with the previous simulation studies. In a different study, Sliwinska-Bartkowiak *et al.*[17] studied the effect of confining CCl_4 in silica-based pores (CPG and VYCOR) that have a rather weak fluid-wall interaction, and observed a depression of the melting temperature. These experimental studies provided an overall picture of the effect of the fluid-wall interaction on the melting of confined CCl_4, drawing a parallel with the simulation study of Miyahara and Gubbins. In order to further elucidate the effect of the pore-wall interaction it is necessary to understand the inhomogeneity of the fluid structure in the confined space. In the free energy study by Radhakrishnan and Gubbins of LJ methane in a graphite slit

pore,[22] the presence of a thermodynamically stable intermediate phase lying between the liquid phase and the solid phase was established in a rigorous manner. The study led to the conclusion that the contact layers (the layers closest to the pore walls) freeze at a higher temperature than the inner layers, and thus the intermediate phase has the structure such that the contact layers are crystalline while the inner layers are liquidlike. The effect of the freezing of the contact layers at an elevated temperature compared to the inner layers causes a significant deviation from the linear behavior predicted by the Gibbs–Thomson equation in the case of smaller pores[24] ($H<5\sigma_{ff}$).

There have been experimental reports that investigated the structure of the confined phases through NMR and x-ray diffraction techniques. Overloop and Van Gervan[14] studied freezing of water in porous silica using NMR, and they suggest that in the confined solid phase up to three molecular layers adjacent to the pore wall (which they term ''bound water'') have a structure that is different from the crystal phase and from that of the free liquid. The rest of the water molecules in the pore interior were in the form of cubic ice (I_c) and the freezing temperatures were consistent with the Gibbs–Thomson equation. Morishige and Nabuoka[12] used x-ray diffraction to study water in siliceous MCM-41 having a range of pore sizes, and also confirmed the existence of a disordered layer of water molecules near the pore wall, with the inner region being the I_c phase. Morishige and Kawano[13] also studied water in Vycor glass and found evidence for both the cubic I_c phase as well as the ordinary hexagonal (I_h) phase. Baker *et al.*[15] studied the nucleation of ice in sol-gel silicas and MCM-41 and found that the crystal structure depends strongly on the conditions and nature of the porous material, showing characteristics of both I_h and I_c forms. Morishige and Kawano[13] have reviewed other experimental studies of the freezing/melting behavior of water in porous silicas and glasses.

In a recent study, Booth and Strange[16] examined the melting of cyclohexane in porous silica using the NMR technique. The melting temperature was below the bulk melting point, and in the confined solid phase there were two distinct components of the transverse relaxation time. The short component (15–30 μs, comparable to the crystal phase in the bulk) was attributed to the crystal phase in the interior of the pore, and the long component was attributed to a liquidlike contact layer (the layer adjacent to the pore walls). Further lowering of temperature led to the freezing of the surface (contact) layer as well.

Sliwinska-Bartkowiak and co-workers attempted to characterize the melting/freezing transition for a dipolar fluid, nitrobenzene confined in controlled pore glass of different pore sizes, using DSC and dielectric relaxation spectroscopy.[17] The depression in the melting temperature followed the Gibbs–Thomson equation for pore sizes larger than 7.5 nm; however, significant deviation was observed for a smaller pore width. The results from both experiments were in good agreement. The authors also made a quantitative estimate of the rotational relaxation time in the fluid and crystal phases by fitting the complex permittivity $\epsilon^* = \epsilon'(\omega) - i\epsilon''(\omega)$ measurements to the Debye dispersion equation. In addition to the liquid and crystal phase relaxation, a third relaxation component was observed, that supported the existence of a contact layer with dynamic properties that were more liquidlike, and different from the inner layers as found in the previous studies.

The experimental studies involving x-ray diffraction as well as NMR methods, and the simulation studies involving free energies, establish the presence of a stable intermediate inhomogeneous confined phase that has important consequences for the nature of the phase transition, as well as the shift in the freezing temperatures. Experiments done on silica based pores (weaker wall-fluid interaction)[17,25] conclude that the contact layers freeze at a lower temperature than the inner layers while the simulation studies involved graphite pores (strong wall-fluid interaction) predict that the contact layers freeze at an elevated temperature compared to the inner layers.

In this paper, we use an order parameter formalism combined with Landau theory[22] to investigate the effect of varying pore width, fluid–fluid and fluid–solid interactions on the shift in the freezing temperature, the presence or absence of a contact layer phase and the structure of these phases. Based on these calculations we develop a global freezing diagram that predicts the freezing behavior for a variety of fluids in common porous systems.

II. METHODS

A. Simulation

We performed grand canonical Monte Carlo (GCMC) simulations of Lennard-Jones methane adsorbed in slit-shaped pores of width $H=7.5\sigma_{ff}$, H being defined as the perpendicular distance between the planes passing through the nuclei of the first layer of molecules that make up the pore walls of the slit-shaped pore. The interaction between the adsorbed fluid molecules is modeled using the Lennard-Jones (12,6) potential with size and energy parameters chosen to describe methane ($\sigma_{ff}=0.381$ nm, $\epsilon_{ff}/k_B=148.1$ K). The pore walls are modeled as a continuum of LJ molecules using the''10-4-3'' Steele potential[26,27] given by

$$\phi_{fw}(z)=2\pi\rho_w\epsilon_{fw}\sigma_{fw}^2\Delta\left[\frac{2}{5}\left(\frac{\sigma_{fw}}{z}\right)^{10}-\left(\frac{\sigma_{fw}}{z}\right)^{4}-\left(\frac{\sigma_{fw}^4}{3\Delta(z+0.61\Delta)^3}\right)\right]. \quad (1)$$

Here, the σ's and ϵ's are the size and energy parameters in the Lennard-Jones (LJ) potential, the subscripts f and w denote fluid and wall, respectively, Δ is the distance between two successive lattice planes of graphite, z is the coordinate perpendicular to the pore walls and k_B is the Boltzmann's constant. For a given pore width, H, the total potential energy from both walls is given by

$$\phi_{\text{pore}}(z)=\phi_{fw}(z)+\phi_{fw}(H-z). \quad (2)$$

The strength of attraction of the pore walls relative to the fluid-fluid interaction is determined by the coefficient $\alpha = (\rho_w\epsilon_{fw}\sigma_{fw}^2\Delta)/\epsilon_{ff}$ in Eq. (1). Throughout the study the

TABLE I. Summary of pore models and freezing temperatures.

Pore-Wall Model	Wall Strength, α	T_f/K, contact layers	T_f/K, inner layers
Bulk			101.4
Model 1	0	–	48.0
Model 2	0.34	66.0	74.0
Model 3	0.68	78.0	86.0
Model 4	0.85	109.0	103.0
Model 5	1.65	120.0	109.0
Model 6	2.14	123.0	113.9

fluid–fluid interaction was kept fixed and the parameters for the wall potential were varied. Six different sets of parameters were chosen for pore-wall interaction that ranged from a purely repulsive wall to a strongly attractive wall; see Table I.

The simulation runs were performed in the grand canonical ensemble, fixing the chemical potential μ, the volume V of the pore and the temperature T. The dimensions of the rectilinear simulation cell were $10\sigma_{ff}\times 10\sigma_{ff}\times H$ for the most part of the study, however, we also performed a system size scaling study that involved system sizes as large as $40\sigma_{ff}\times 40\sigma_{ff}\times H$. The system typically contained up to 700 adsorbed molecules (up to 12 000 molecules for the case of the largest system used in the system size scaling analysis). Periodic boundary conditions were employed in the two dimensions defining the plane of the pore walls. The simulation was set up such that insertion, deletion and displacement moves were attempted with equal probability, and the displacement step was adjusted to have a 50% probability of acceptance. Thermodynamic properties were averaged over 100–1000 million individual Monte Carlo steps. The length of the simulation was adjusted such that a minimum of 50 times the average number of particles in the system would be inserted and deleted during a single simulation run. We note that the geometry of the simulation box in our study is not commensurate with the crystal structure in the confined solid phase. However, it was ensured that the simulation box size was large enough to avoid any artifacts due to the incommensurability between the shape of the simulation box and the crystal structure.[24]

B. Free energy

The method to calculate the free energy relies on the calculation of the Landau free energy as a function of an effective bond orientational order parameter, Φ, using GCMC simulations. The Landau free energy is defined by[28]

$$\Lambda[\Phi] = -k_B T \ln(P[\Phi]) + \text{constant}, \tag{3}$$

where $P[\Phi]$ is the probability of observing the system having an order parameter value between Φ and $\Phi+\delta\Phi$. The probability distribution function $P[\Phi]$ is calculated in a GCMC simulation by collecting statistics of the number of occurrences of a particular value of Φ in the form of a histogram, with the help of umbrella sampling.[29] For a particular phase, for instance phase A, the grand free energy Ω_A is related to the Landau free energy by

$$\exp(-\beta\Omega_A) = \int_{\Phi_{\min,A}}^{\Phi_{\max,A}} d\Phi \exp(-\beta\Lambda[\Phi]). \tag{4}$$

The grand free energy at a particular temperature can be calculated by numerically integrating over the order parameter range $(\Phi_{\min,A}-\Phi_{\max,A})$ that corresponds to the particular phase A in consideration. More complete details of the method for confined systems are given elsewhere.[22,30,31]

We use a two-dimensional order parameter previously introduced by Mermin[32] to characterize the order in each of the molecular layers:

$$\Phi_j = \left| \frac{1}{N_b} \sum_{k=1}^{N_b} \exp(i6\theta_k) \right| = |\langle \exp(i6\theta_k) \rangle_j|. \tag{5}$$

Φ_j measures the hexagonal bond order within each layer j. Nearest neighbors in the same layer of a given molecule were identified as those molecules that were less than a cutoff distance r_{nn} away. We used a cutoff distance $r_{nn}=1.3\sigma_{ff}$, corresponding to the first minimum in the $g(r)$ function. Each nearest neighbor bond has a particular orientation in the plane of the given layer, with respect to a reference axis, and is described by the polar coordinate θ. The index k runs over the total number of nearest neighbor bonds N_b in layer j. The overall order parameter Φ is an average of the hexagonal order in all the layers:

$$\Phi = \left(\sum_{j=1}^{N_{\text{layers}}} \Phi_j \right) \Big/ N_{\text{layers}}. \tag{6}$$

For molecules with isotropic interaction potential the only two-dimensional closed packed structure is the hexagonal crystal. The quantity Φ is invariant under rotation about the z axis. We expect $\Phi=0$ when all the layers have the structure of a two-dimensional liquid, $\Phi=1$ in the solid phase and $0<\Phi<1$ in the orientationally ordered hexatic phase.

C. Dielectric relaxation spectroscopy

The capacitance, C, and the tangent loss, $\tan(\delta)$, of the capacitor filled with nitrobenzene between the plates were measured in the frequency range, ω between 1 Hz and 10 MHz, for various temperatures.[17] For the case of nitrobenzene confined in activated carbon fibers (ACF), the sample was introduced between the capacitor plates as a suspension of porous particles in pure nitrobenzene. The contributions to the complex relative permittivity $\kappa^*=\kappa'-i\kappa''$ were determined. The electrodes were blocked using a dielectric (teflon) for samples containing the ACF, as the suspension was conducting. The Debye dispersion relation for an isolated dipole rotating in a viscous medium under alternating electric field was used to calculate the orientational relaxation time from the premittivity dispersion spectrum.[17]

III. RESULTS

A. Phase behavior

The Landau free energy for the confined methane was calculated as a function of the order parameter Φ for different temperatures and different pore models. The different phases are identified by the different minima in the Landau

free energy curves. Each phase is characterized by calculating the average value of the order parameter and the two-dimensional, in-plane pair correlation functions in each of the molecular layers by constraining the phase space trajectory such that only configurations whose average value of the order parameter lie in the range $\Phi_{\mathrm{min,phase}}$ and $\Phi_{\mathrm{max,phase}}$ of the particular phase in consideration, is sampled. The calculated averages and pair correlation functions are insensitive to the exact values of $\Phi_{\mathrm{min,phase}}$ and $\Phi_{\mathrm{max,phase}}$ chosen, as both of them will lie close to the corresponding local maximum in the Landau free energy function. The region around the local maximum in the Landau free energy corresponds to low probability configurations that have negligible contributions to the average value of the thermodynamic property in question.

The systems studied here are summarized in Table I. The Landau free energy functions are plotted for four different models of the pore walls in Fig. 1. The minimum that occurs at the values of order parameter near zero corresponds to the liquid phase. The minimum close to an order parameter value of 1.0 corresponds to the crystalline phase. For certain pore models an intermediate phase lies between the liquid and the crystalline phase. The temperature in each case is chosen such that the free energy difference between the intermediate phase and the liquid phase or the crystalline phase (which ever has a lower free energy) Δ_{min} is a minimum:

$$\Delta_{\mathrm{min}} = \mathrm{Min}\{\Omega_{\mathrm{int}} - \Omega^*\}_T,$$
$$\Omega^* = \Omega_{\mathrm{cry}} \quad \text{if} \quad \Omega_{\mathrm{cry}} < \Omega_{\mathrm{liq}}, \tag{7}$$
$$\Omega^* = \Omega_{\mathrm{liq}} \quad \text{if} \quad \Omega_{\mathrm{liq}} < \Omega_{\mathrm{cry}}.$$

In Eq. (7) ''liq,'' ''cry'' and ''int'' refer to liquid, crystal and intermediate phases, respectively, and the function $\mathrm{Min}\{f\}_T$ minimizes f with respect to T.

For repulsive and weakly attractive walls, the intermediate phase is at best metastable. For strongly attracting walls, the intermediate phase exists as a thermodynamically stable phase for a certain range of temperatures. The plot of Δ_{min} versus the relative strength of the fluid-wall to the fluid–fluid interaction α is shown in Fig. 2. For values of α less than 0.48, Δ_{min} is always positive, and thus only two thermodynamically stable phases exist, liquid and crystalline. For values greater than 0.48, three stable phases exist in the system. For the case of the purely repulsive pore, the disordered phase exists as a three-dimensional liquid and the ordered phase is a fcc crystal. The increase in the α value for the pore model induces layering in the system, distinct molecular layers forming parallel to the plane of the pore walls. In these cases the individual molecular layers exist as a quasi-two-dimensional liquid in the disordered phase and as two-dimensional hexagonal crystal in the crystalline phase. The intermediate phase is a partially ordered phase. In the case of a weakly attractive pore, the contact layers (i.e., the layers adjacent to the two pore walls) are liquidlike while the inner layers are crystalline [see Fig. 3(a)]; thus the contact layers freeze at a lower temperature compared to the inner layers. For the case of a strongly attractive pore, the intermediate phase is characterized by crystalline contact layers and liquidlike inner layers; in this case the contact layers freeze at a

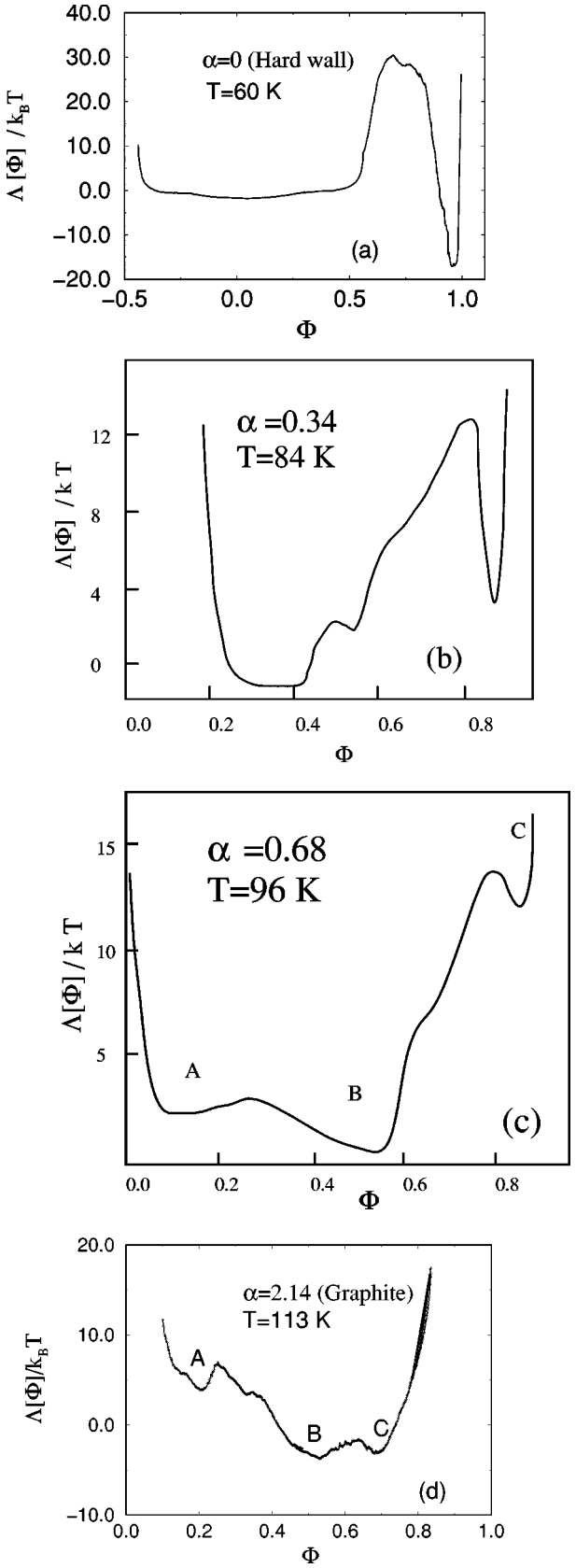

FIG. 1. The Landau free energy as a function of the order parameter for LJ methane in four different pore models: (a) $\alpha = 0$ at $T = 60$K; (b) $\alpha = 0.34$ at $T = 84$ K; (c) $\alpha = 0.68$ at $T = 96$ K; (d) $\alpha = 2.14$ at $T = 113$ K.

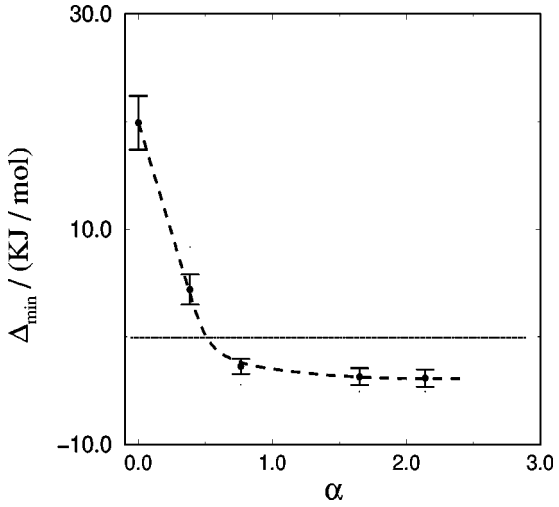

FIG. 2. The plot shows $\Delta_{\min}$ as a function of α. Regions with negative values of $\Delta_{\min}$ correspond to the presence of a thermodynamically stable intermediate phase in the system.

higher temperature compared to the inner layers [Fig. 3(b)]. The reversal of the freezing behavior of the contact layers occurs for α values between 0.85 and 1.15. The crossover of the branches of the grand free energy of the liquid, intermediate and the crystal phases determines the freezing temperature of the contact layers as well as the inner layers. The values of the freezing temperature as a function of the strength of the fluid-wall interaction parameter α are summarized in Table I. The bulk freezing temperature of LJ methane is 101.4 K. It is also observed that for weakly attractive pores ($\alpha<0.85$) there is a depression in the freezing temperature and for strongly attractive pores ($\alpha>1.15$) there is an elevation in the freezing temperature, when compared to the bulk.

For a LJ fluid confined in a slit pore having a continuum ''10-4-3'' potential walls, the configurational partition function in the canonical ensemble $Q_{\text{config}}(N,V,T)$, is given by

$$Q_{\text{config}}=\int_0^V d\mathbf{r}_i^N \exp\left(-\frac{1}{T^*}f(\mathbf{r}_i^N)-\frac{\alpha}{T^*}g(\mathbf{r}_i^N)\right), \qquad (8)$$

where the integration is over all $\mathbf{r}_i$, i.e., $\mathbf{r}_1,\mathbf{r}_2,\mathbf{r}_3$, etc., N is the number of molecules in the system, V is the volume of the system, $\mathbf{r}_i$ represents the spatial coordinates of molecule i, ''f'' accounts for the fluid–fluid interaction and ''g'' accounts for the fluid-wall interaction. Thus,

$$Q_{\text{config}}=Q_{\text{config}}[N,V^*,T^*,\alpha,\sigma_{ff},\sigma_{fw}]. \qquad (9)$$

Typical fluid and pore systems have similar σ_{ff} and σ_{fw} values for small adsorbate molecules, and for a narrow range of these size parameters, g is a weak function of σ_{ff} and σ_{fw}. Thus, from the principle of corresponding states,[33] to a good approximation for small adsorbates,

$$\Lambda^*\approx\Lambda^*[N,V^*,T^*,\alpha,H^*] \qquad (10)$$

and

$$T_f^*\approx T_f^*[\alpha H^*].$$

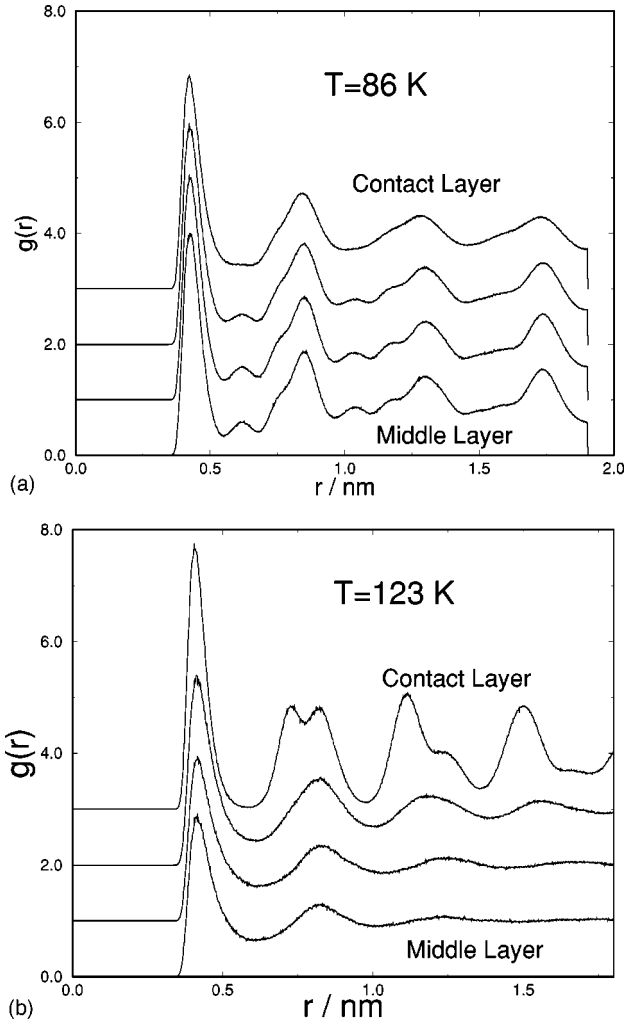

FIG. 3. (a) Plot shows 2-D, in-plane pair correlation functions in the molecular layers corresponding to the intermediate phase for LJ methane in a weakly attractive pore ($\alpha=0.68$, $T=86$ K). (b) The same for LJ methane in a strongly attractive pore ($\alpha=2.14$, $T=123$ K).

For a LJ fluid confined in a model slit pore with ''10-4-3'' potential, Eq. (10) implies that the complete phase behavior including the freezing temperature is predictable from the knowledge of the Landau free energy as a function of the order parameter and temperature. The value of α together with results such as those in Fig. 1, in reduced variables, can be used to predict the freezing properties of the particular LJ system under consideration.

In order to predict the freezing properties of realistic fluid/pore systems, the respective fluid–fluid and fluid-wall interactions are approximated using the LJ potential and the slit pore model. The LJ parameters for the fluid are chosen to reproduce thermophysical data (second virial coefficients or viscosity) of the bulk gas. The pore model parameters, $\sigma_{ww},\epsilon_{ww},\rho_w$ and Δ, are chosen such that molecular simulation results of adsorption of LJ nitrogen matches the experimental results at 77 K. Based on the fitted potential parameters, the calculated value of α is used to predict the freezing temperatures of the contact layers as well as that of the inner layers, and also the structure of the confined fluid in various phases. Three different categories of fluids were chosen:

TABLE II. Potential energy parameters for fluid–fluid interactions.

Fluid	LJ parameters σ_{ff}/nm, $\epsilon_{ff}/(k_BK)$	Property fitted
Simple fluids		
Ar	3.4, 119.8	2nd Viral Coeff.
Kr	3.6, 171.0	2nd Viral Coeff.
Xe	4.1, 222.0	2nd Viral Coeff.
N_2	3.7, 96.0	2nd Viral Coeff.
CH_4	3.8, 148.1	2nd Viral Coeff.
CO_2	4.4, 192.0	2nd Viral Coeff.
CCl_4	5.1, 366.0	Freezing point
Dipolar fluids		
HCl	3.3, 360.0	Viscosity
HI	4.1, 324.0	Viscosity
$C_6H_5NO_2$	5.7, 425.0	Freezing point
H-bonding fluids		
NH_3	2.6, 711.0	2nd Viral Coeff.
H_2O	3.2, 888.0	2nd Viral Coeff.

TABLE III. Fluid–fluid interaction parameters used to calculate the fluid-wall interactions.

Fluid	Model	Parameters
Simple fluids		σ_{ff}/nm, $\epsilon_{ff}^{\text{dispersive}}/(k_BK)$
Ar	LJ	3.4, 119.8
Kr	LJ	3.6, 171.0
Xe	LJ	4.1, 222.0
N_2	LJ	3.7, 96.0
CH_4	LJ	3.8, 148.1
CO_2	LJ	4.4, 192.0
CCl_4	LJ	5.1, 366.0
Dipolar fluids		σ_{ff}/nm, $\epsilon_{ff}^{\text{dispersive}}/(k_BK)$, μ/Debye
HCl	Stockmayer	3.3, 327.0, 1.03
HI	Stockmayer	4.1, 324.0, 0.1
$C_6H_5NO_2$	Stockmayer	5.7, 265.0, 4.2
H-Bonding fluids		
NH_3	Stockmayer	2.6, 320.0, 1.5
H_2O	SPC-E	3.2, 75.0, charges

simple fluids, dipolar fluids and hydrogen bonding fluids. The LJ parameters that represent the fluid–fluid interaction for these fluids are given in Table II. For dipolar and hydrogen bonding fluids the approximation of the fluid–fluid interaction by a LJ potential is a drastic one, however, the predicted freezing behavior is expected to be qualitatively correct. Two different models of slit pores are considered: a strongly attractive pore with interaction parameters chosen to model graphitic carbon pores, and a weakly attractive pore modeled on silica walls. The size parameter σ_{fw} to be used in the 10-4-3 potential is taken to be $(\sigma_{ff}+\sigma_{ww})/2$. For simple fluids, the energy parameter ϵ_{fw} is calculated as $(\epsilon_{ff}\epsilon_{ww})^{0.5}$, consistent with the Lorentz–Berthlot mixing rule. For dipolar and hydrogen bonded fluids, the LJ fluid–fluid parameters given in Table II include, in some approximate, averaged fashion, the effects of direct electrostatic and induction interactions. The use of the ϵ_{ff} values given in Table II in the Lorentz–Berthelot rule, $(\epsilon_{ff}\epsilon_{ww})^{0.5}$, to estimate ϵ_{fw} is therefore not appropriate. We expect direct electrostatic and induction interactions between such fluid molecules and the wall to be small, and we therefore neglect them. The LJ fluid-wall energy parameter is taken to be

$$\epsilon_{fw}=(\epsilon_{ff}^{\text{dispersion}}\times\epsilon_{ww})^{1/2}, \tag{11}$$

where $\epsilon_{ff}^{\text{dispersion}}$ is the LJ parameter value that represents only the dispersion contribution. For HCl, HI, $C_6H_5NO_2$ and NH_3, the values of $\epsilon_{ff}^{\text{dispersion}}$ fitted to the Stockmayer potential[34] were used in Eq. (11), while for H_2O the value fitted to the SPC-E model was used. These values are given in Table III. Interaction parameters that characterize the pore walls are given in Table IV.

The global freezing diagram for typical fluid/pore systems is given in Fig. 4. Each fluid is placed on the vertical axis depending on the porous material in which it is confined and the α value. The systems that lie in region 1 ($\alpha>1.15$) show an elevation in the freezing point and are characterized by an intermediate phase with frozen contact layers and fluidlike inner layers. Systems with larger values of α have a larger elevation in freezing temperature. The systems that lie in region 2 ($0.5<\alpha<0.85$) show a depression in the freezing point behavior and have an intermediate phase with fluid-like contact layers and frozen inner layers. The systems that lie in region 3 ($\alpha\leqslant 0.5$) also show a depression in freezing point but they are characterized by an intermediate phase that is metastable. Thus, these systems have only two true thermodynamic phases (liquid and crystalline solid). In regions 2 and 3, smaller values of α lead to larger magnitude of the depression in the freezing temperature. The dashed line represents the boundary between regions 2 and 3. The boundary that separates regions 1 and 2 extends between the two dotted lines. Thus, systems falling in this boundary region can either show a depression or an elevation in the freezing temperature on confinement but the magnitude of the shift will be close to zero.

IV. DISCUSSION

The global freezing diagram (Fig. 4) predicts the freezing temperatures of the contact and the inner layers and the confined fluid structure in the different phases for a variety of fluids in slit pores with model parameters to suit silica and graphite interactions. It is clear that the strength of the fluid-wall interaction relative to the fluid–fluid interaction (α) plays a very important role in determining the freezing temperature as well as the structure of the confined fluid. The estimates of the freezing temperature for many systems are to be regarded as approximate, because of the simplicity of the pore models and the interaction potentials used to predict the phase diagram. Comparison between simulation and experiment is expected to be in nearly quantitative agreement

TABLE IV. Potential energy parameters for the pore walls.

Pore-Wall Model	σ_{ff}/Å, $\epsilon_{ww}/(k_BK)$	$\rho_s\sigma_{ww}^3$, Δ/Å
Graphite	3.81, 28.0	2.5, 3.3
Silica	2.7, 230.0	0.87, 2.2

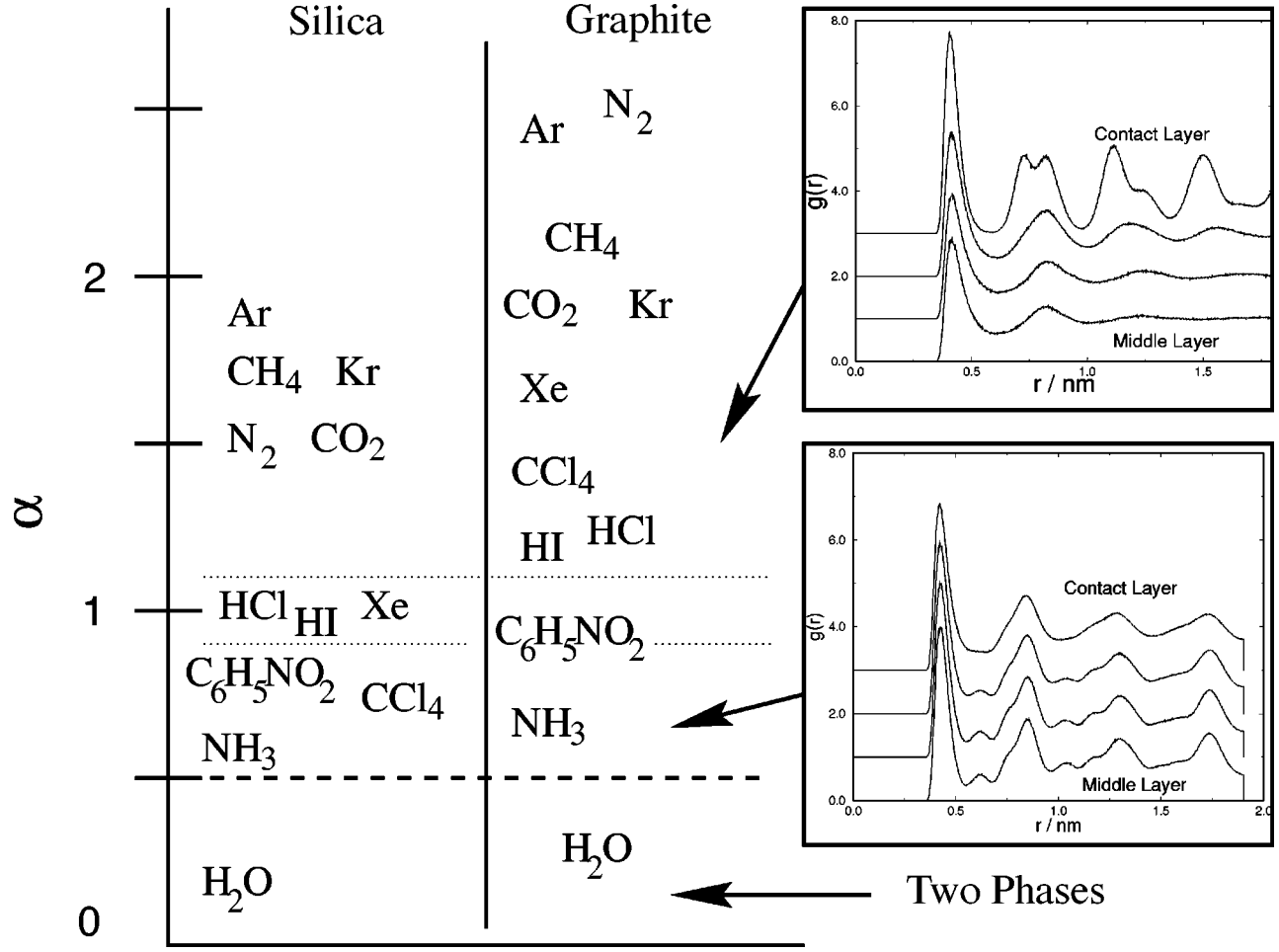

FIG. 4. The figure represents the global freezing diagram for typical fluids confined in silica and graphite based pores. The different regions in the plot have different phase behavior. Fluid-pore systems that belong to region 1 ($\alpha > 1.15$) show an elevation in freezing temperature when compared to the bulk, while those in regions 2 ($0.5 < \alpha < 0.85$) and 3 ($\alpha \leq 0.5$) show a depression in freezing temperature. The pair correlation function plots show the fluid structure of the intermediate phase corresponding to the particular region.

for the case of simple fluids in graphite pores, for which the pore model and interaction potentials are best suited. In the case of polar and H-bonding fluids, approximating the fluid–fluid potential as LJ can lead to quantitative differences; however, we expect qualitative agreement with experiment. For the case of silica based pores, the freezing temperature in Fig. 4 is expected to be an overestimation of the actual experimental values, as most silica based porous materials (CPG, VYCOR, MCM-41, etc.) have cylindrical pore geometry instead of slit pore geometry. The additional confinement due to the cylindrical geometry has the same effect as reduction in α values, due to additional steric constraints on the formation of the confined crystal phase.[20,25]

Experimental studies have been reported that confirm the predictions of the global freezing diagram. Radhakrishnan *et al.*[23,24] studied freezing of CCl_4 in activated carbon fibers using differential scanning calorimetry, and observed a large increase (57 K) in the freezing temperature of the confined fluid compared to the bulk, which is consistent with the predictions of Fig. 4. Other experimental reports on freezing of CCl_4 in CPG and VYCOR pores (silica glasses) using DSC[17] find a depression in the freezing temperature when compared to the bulk. These trends are consistent with the weak potential of interaction experienced by the CCl_4 molecules due to the silica walls, and agree qualitatively with the predictions of the global phase diagram. The authors also studied freezing of nitrobenzene in silica based pores using dielectric relaxation spectroscopy (DS)[17] and found similar trends on the depression of the freezing temperature, which again confirms to the predictions of the global phase diagram. In addition to the freezing temperature, the DS measurements of the rotational relaxation times of the dipolar molecules also showed that the contact layers have different dynamic and structural properties compared to the pore interior. The authors found that the freezing temperature of the contact layers (as measured by the jump in the value of the dielectric relaxation time) was less than that of the inner layers (as measured by the jump in the value of the dielectric constant[25,36]). This behavior implies that the structure of the confined intermediate phase in the silica based pores is the same as that of the intermediate phase described by Fig. 3(b). Following the study of Sliwinska-Bartkowiak *et al.*,[17] we performed dielectric relaxation spectroscopy studies on the freezing of nitrobenzene in activated carbon fibers. Due to the conducting nature of the pore material, the electrodes were blocked us-

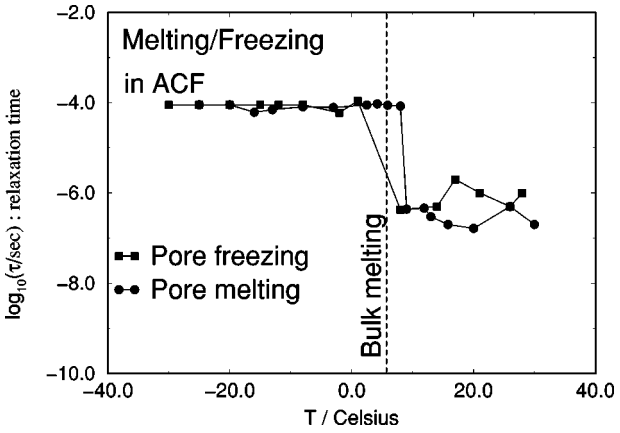

FIG. 5. Relaxation time as a function of temperature for bulk nitrobenzene and nitrobenzene confined in activated carbon fibers.

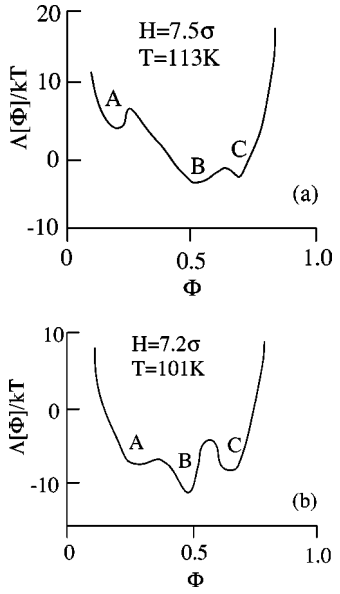

FIG. 6. Landau free energy curves for methane confined in a graphite pore of two different pore widths: (a) $H=7.5\ \sigma_{ff}$ and (b) $H=7.2\ \sigma_{ff}$.

ing a thin film of teflon before studying the frequency response. The experimental procedure is outlined in Sec. II C, and in more detail in Ref. 17. A plot of the dielectric relaxation times as a function of temperature is shown in Fig. 5 for nitrobenzene confined in the micropores of the ACF material. The bulk melting temperature for nitrobenzene is 5.6 °C and is denoted by the dashed vertical line. For the confined fluid, the corresponding freezing and melting temperatures are 3 °C and 8 °C, respectively, as seen from the discontinuities in values of the dielectric relaxation times during the freezing and melting runs. We can therefore conclude that the shift in the freezing temperature due to confining the nitrobenzene molecules in ACF is nearly zero in the experiments, which is consistent with the predictions of Fig. 4. Figure 4 shows that the nitrobenzene/graphite system lies in the boundary of regions 1 and 2, and is therefore expected to have a very small shift if any in the freezing temperature due to confinement. We note that the relaxation times for the liquid in the confined system is much larger than the typical bulk liquid, because the measured relaxation time is that of the contact layers of nitrobenzene that experience a deep potential energy well due to the pore walls and hence are in a orientationally ordered hexatic state.[22,35] The relaxation times for the inner layers in their liquid state are in the range of nano-seconds, and are outside the frequency range of our measurements. On freezing, the crystalline phase relaxation in the bulk as well as in the pore are of the order of milli-seconds.[17,36]

Experimental studies performed using the surface force apparatus are most suited for direct comparison with the predictions of the global phase diagram. The surface force apparatus consists of two parallel plates with mica surfaces in which the spacing between the mica surfaces can be controlled at the scale of an angstrom or less. Such a system can be modeled using the slit pore approximation as we have done in our study. Klein and Kumacheva[37] studied freezing of cyclohexane between parallel mica surfaces (slit shaped geometry) and observed a significant increase in the melting temperature on confinement. There has been contradicting reports on the nature of the shift in the freezing temperature of cyclohexane between parallel mica surfaces in a surface force apparatus.[38] However, a recent simulation study[39] based on the experimental system of Klein and Kumacheva, also predicted an elevation in the freezing temperature. The model parameters used to mimic the mica interaction in the study[39] yielded an α value of 2.47 for cyclohexane confined between the mica surface, which falls in region 1 in the global phase diagram (Fig. 4), consistent with the elevation in the freezing temperature. A more convincing evidence that supports the verification of the global phase diagram is based on the experimental study of Watanabe *et al.*,[40] which reported an elevation of freezing temperature for benzene confined in activated carbon fibers. The α value for a LJ benzene (fitted to reproduce the melting point of benzene in the bulk) in graphite is 2.15; thus, the freezing temperature elevation is again consistent with the global phase diagram.

The simulation results reported in Figs. 1–4 are for a fixed pore width H of $7.5\sigma_{ff}$. As the pore width is reduced the confinement effect on the freezing behavior is enhanced. In addition, there is an effect due to variation in the inter-layer distance (average distance between the confined molecular layers), which depends on the pore width H. The ease with which the fluid freezes in the pore and the extent of the hysteresis loops depend crucially on the inter-layer separation d; Refs. 19,22,24,41. For $d/\sigma_{ff} \geqslant 0.95$ the fluid freezes into a defect free crystal in our simulations, with hysteresis loops observed during adsorption and desorption spanning 2–10 K. The defects in the crystal structure increase in the range $0.90 \leqslant d/\sigma_{ff} \leqslant 0.95$, with the extent of hysteresis loops increasing to about 10–30 K; the thermodynamic freezing temperature of the inner layers decreases as d decreases. For $d \leqslant 0.90$, the inner layers of the confined fluid *do not* undergo a freezing transition. Thus, the thermodynamic freezing temperature is not a smooth function of pore width and shows oscillatory behavior because of its crucial dependence on d. There are windows of pore widths where the fluid does not freeze because of the lower bound in the value of $d = 0.90\sigma_{ff}$ that supports freezing.[24] Figure 6 shows the Lan-

dau free energy curves for LJ methane in two graphite pores which have the same number of confined molecular layers but different values for the inter-layer separation d, i.e., slightly different pore widths. The hysteresis loops resulting from the freezing and melting curves are very different for the different pore widths (about 8 K for the $7.5\sigma_{ff}$ pore, and about 25 K for the $7.2\sigma_{ff}$ case). It is evident from the Landau free energy plots that the barrier to nucleation in Fig. 6(b) is much larger than in Fig. 6(a). The obvious explanation is that the steric hindrance for the formation of the confined crystal phase is much larger in the slightly smaller pore. The extent of the hysteresis loops depends on the temperature span between the limit of metastability of the melting and freezing processes, i.e., the difference in temperatures between the state point at which the minimum corresponding to the liquid phase turns into a shoulder, and the state point at which the minimum corresponding to the crystalline phase becomes a shoulder. From Fig. 6 it is clear that the free energy fluctuation required to nucleate a new phase within an existing phase is greater for the slightly smaller pore width and hence the temperature span between the limits of metastability of the liquid phase and the crystalline phase is correspondingly large; it is also evident that the thermodynamic melting/freezing transition temperature for the $7.2\sigma_{ff}$ pore (which is close to 101 K) is less than for the $7.5\sigma_{ff}$ pore (which is 113 K). Since the real porous material is networked and has a pore size distribution,[24,42,43] the freezing transition tends to be smeared out (less sharp) because of the effect the interlayer separation has on the freezing temperature, $T_f(H)$. Other factors that have been neglected in our model are the anisotropic polarizability of the graphite walls,[44] which is expected to have a negligible effect on the interaction energy for simple fluids, it can account for 5%–10% of the fluid-wall potential energy for strongly dipolar molecules such as water.

In conclusion we comment on the methodology used to calculate the freezing temperature and characterize the phase behavior. The Landau free energy formalism was used to calculate the grand free energy of the fluid and crystalline states as a function of temperature, for LJ CCl_4 confined in slit-shaped pores. The free energy difference between the ordered and the disordered state is directly calculated. In addition to the free energy, a quantitative estimate of the free energy barrier to nucleation is obtained, although such a quantity is sensitive to system size effects. However, the absolute value of the free energy difference is only a weak function of system size, and is estimated to an accuracy of $1k_BT$, as shown by Lynden-Bell *et al.*[31] The exact location of the equilibrium transition temperature by free energy calculation is an improvement over methods that use the jump in density to locate the freezing/melting points in terms of accuracy, as it is independent of the width of the hysteresis loops. Previously existing methods to calculate the free energy of a confined solid phase in simulations are all based on thermodynamic integration.[21,45] This method involves a numerical integration of the Gibbs free energy starting from a known reference phase (the Einstein crystal for the solid phase and the ideal gas for the liquid phase) to the state point of interest. It relies on finding a suitable path of integration which is thermodynamically reversible, i.e., the path does not intersect any phase boundary characterized by a first order transition. Thus, the free energy study in Ref. 21 was limited to confined systems with repulsive or weakly attractive wall-fluid potentials (pore models for which $\alpha<0.48$ so that the intervening intermediate phase is never a thermodynamically stable phase, hence the path of integration does not run into a first order phase transition). For the more ubiquitous case of a wall-fluid potential that is moderately or strongly attractive ($\alpha>0.48$), this method breaks down. This is because the intermediate phase becomes a thermodynamically stable phase. This makes it impossible to find a reversible path from the ideal gas phase to the fluid phase, since any such path runs into a first order transition leading to the formation of the intervening intermediate phase. Thus one should exercise great caution in using the thermodynamic integration methods in confined systems (or inhomogeneous systems in general) because of the subtle phase transitions driven by the external potential that lead to formations of inhomogeneous phases that are thermodynamically stable. Such problems are circumvented by the use of the order parameter formulation and the Landau approach.

The level of the Landau theory used in this study is still an approximation as it does not allow the order parameter to be explicitly spatially inhomogeneous. Instead, an average order parameter is used that takes into account the spatial fluctuations at a crude level but does not take into account the orientational fluctuations in the order parameter. In this sense, the field theoretic method used in this study comes under the general class of mean field approximations. This approximation is expected to give reliable and quantitative correct results in studying crystalline phases in which there is a very strong coupling between the phase of the orientational order parameters in different molecular layers [since the order parameter Φ in Eq. (5) is a complex number, it has a magnitude as well as a phase associated with it]. This prevents spatial variations in the phase of the orientational order parameter. However, when studying other systems with hexatic order, the level of mean field theory used here fails to capture the spatial variations in the phase of the order parameter. In such cases a more generic form of the order parameter formalism (the Landau–Ginzburg approach) is more appropriate, as the free energy can be calculated as a function of the spatially varying order parameter.[46,35] The other main approximation in the methodology is the use of corresponding states theory in relation to freezing transitions. Although this principle is valid for the LJ model systems that we have used in this study, it should be noted that the global freezing diagram (Fig. 4) is based on Eq. (10), which is derived on the assumption that the Landau free energy function is a weak function of the LJ size parameters. Thus, the global freezing diagram is not expected to work very well for predicting the freezing temperatures of large molecules like butane and higher alkanes (nor for any other functional derivatives of these large molecules like alcohols, amines, etc.).

The corresponding states theory is known not to work as well with freezing transitions as with vapor–liquid transitions in real laboratory systems. The primary reason for the poor performance of the corresponding states theory for

freezing transitions is the importance of three body effects in the formation of the crystalline phase; this is not captured by simple two-parameter models like Lennard-Jones.[47] However, the qualitative trends we have obtained from such a principle are still reliable, as the predictions are consistent with numerous experimental studies.

ACKNOWLEDGMENTS

It is a pleasure to thank Katsumi Kaneko and Minoru Miyahara for helpful discussions. This work was supported by grants from the National Science Foundation (Grant No. CTS-9896195) and KBN (Grant No. 2 PO3B 175 08), and by a grant from the U.S.–Poland Maria Sklodowska-Curie Joint fund (Grant No. MEN/DOE-97-314). Supercomputer time was provided under a NSF/NRAC grant (MCA93S011).

[1] J. Warnock, D. D. Awschalom, and M. W. Shafer, Phys. Rev. Lett. **57**, 1753 (1986).
[2] J. L. Tell, H. J. Maris, and G. M. Seidel, Phys. Rev. B **28**, 5122 (1983).
[3] R. H. Torii, H. J. Maris, and G. M. Seidel, Phys. Rev. B **41**, 7167 (1990).
[4] P. E. Sokol, W. J. Ma, K. E. Herwig, W. M. Snow, Y. Wang, J. Koplik, and J. R. Banavar, Appl. Phys. Lett. **61**, 777 (1992).
[5] J. H. Strange, M. Rahman, and E. G. Smith, Phys. Rev. Lett. **71**, 3589 (1993).
[6] E. Molz, A. P. Y. Wong, M. H. W. Chan, and J. R. Beamish, Phys. Rev. B **48**, 5741 (1993).
[7] K. M. Unruh, T. E. Huber, and C. A. Huber, Phys. Rev. B **48**, 9021 (1993).
[8] J. A. Duffy, N. J. Wilkinson, H. M. Fretwell, M. A. Alam, and R. Evans, J. Phys.: Condens. Matter **7**, L713 (1995).
[9] E. W. Hansen, M. Stöker, and R. Schmidt, J. Phys. Chem. **100**, 2195 (1996).
[10] K. J. Elder, P. A. Reynolds, F. Trouw, and J. W. White, J. Chem. Soc. Chem. Commun. **1996**, 155.
[11] J. Krim, J. P. Coulomb, and J. Bouzidi, Phys. Rev. Lett. **58**, 583 (1987).
[12] K. Morishige and K. Nobuoka, J. Chem. Phys. **107**, 6965 (1997).
[13] K. Morishige and K. Kawano, J. Chem. Phys. **110**, 4867–4872 (1998).
[14] K. Overloop and L. Van Gerven, J. Magn. Reson., Ser. A **101**, 179 (1993).
[15] J. M. Baker, J. C. Dore, and P. Behrens, J. Phys. Chem. B **101**, 6226 (1997).
[16] H. F. Booth and J. H. Strange, Mol. Phys. **93**, 263 (1998).
[17] M. Sliwinska-Bartkowiak, J. Gras, R. Sikorski, R. Radhakrishnan, L. D. Gelb, and K. E. Gubbins, Langmuir **15**, 6060 (1999).
[18] R. Evans and U. M. B. Marconi, J. Chem. Phys. **86**, 7138 (1987).
[19] M. Miyahara and K. E. Gubbins, J. Chem. Phys. **106**, 2865 (1997).
[20] M. Maddox and K. E. Gubbins, J. Chem. Phys. **107**, 9659 (1997).
[21] H. Dominguez, M. P. Allen, and R. Evans, Mol. Phys. **96**, 209 (1999).
[22] R. Radhakrishnan and K. E. Gubbins, Mol. Phys. **96**, 1249 (1999).
[23] A. Watanabe, K. Kaneko, T. Iiyama, R. Radhakrishnan, and K. E. Gubbins, J. Phys. Chem. B **103**, 7061 (1999).
[24] R. Radhakrishnan, K. E. Gubbins, A. Watanabe, and K. Kaneko, J. Chem. Phys. **111**, 9058 (1999).
[25] M. Sliwinska-Bartkowiak, J. Gras, G. Dydziak, R. Silorski, R. Radhakrishnan, L. Gelb, and K. E. Gubbins, *Proceedings of COPS-V* (Elsevier, Amsterdam, 1999).
[26] W. A. Steele, Surf. Sci. **36**, 317 (1973).
[27] W. A. Steele, *The Interaction of Gases with Solid Surfaces* (Pergamon, Oxford, 1974).
[28] L. D. Landau and E. M. Lifshitz, *Statistical Physics*, 3rd ed. (Pergamon, London, 1980).
[29] G. M. Torrie and J. P. Valleau, Chem. Phys. Lett. **28**, 578 (1974).
[30] J. S. Van Duijneveldt and D. Frenkel, J. Chem. Phys. **96**, 4655 (1992).
[31] R. M. Lynden-Bell, J. S. Van Duijneveldt, and D. Frenkel, Mol. Phys. **80**, 801 (1993).
[32] N. D. Mermin, Phys. Rev. **176**, 250 (1968).
[33] T. M. Reed and K. E. Gubbins, *Applied Statistical Mechanics* (McGraw Hill, New York, 1973).
[34] J. O. Hirshfelder, C. F. Curtiss, and B. Bird, *Molecular Theory of Gases and Liquids* (Wiley, New York, 1964).
[35] R. Radhakrishnan and K. E. Gubbins, pre-print (1999).
[36] R. Radhakrishnan, K. E. Gubbins, M. Sliwinska-Bartkowiak, G. Dydziak, and R. Sikorski, J. Chem. Phys. (submitted).
[37] K. Klein and K. Kumacheva, Science **269**, 816 (1995).
[38] H. K. Christenson, Colloids Surf., A **123**, 355 (1997).
[39] S. T. Cui, P. T. Cummings, and H. D. Cochran, pre-print (1999).
[40] A. Watanabe and K. Kaneko, Chem. Phys. Lett. **305**, 71 (1999).
[41] C. L. Rhykerd, M. Schoen, D. J. Diestler, and J. H. Cushman, Nature (London) **330**, 461 (1987).
[42] L. D. Gelb and K. E. Gubbins, Langmuir **14**, 2097 (1998).
[43] K. T. Thomson and K. E. Gubbins, Langmuir (submitted).
[44] D. Nicholson, Surf. Sci. **181**, L189 (1984).
[45] D. Frenkel and A. J. C. Ladd, J. Chem. Phys. **81**, 3188 (1984).
[46] P. M. Chaikin and T. C. Lubinski, *Principles of Condensed Matter Physics* (Cambridge University Press, Cambridge, 1995).
[47] D. W. Oxtoby, Nature (London) **347**, 725 (1990).